Current Science
CS 5 (5), 5076-5091 (2025)
Received 10 July 2025 | **Revised 15 August** 2025 | **Accepted 20 September** 2025 | **Online Available 26 October** 2025
https://doi.org0/10.52845/CS/2025-5-5-55

Current Science

Current Science

OPEN ACCESS

ISSN(O)2795-8639

Original Article

Assessing the Toxicological Impact of 6PPD-Quinone on Age-Related Cataract: Insights from Network Toxicology and Molecular Docking

Zhuxuan Yan[a,b,c], Hanrui Wang[c], Wei Chi[a,b], Zhenguo Yan[c*]**

[a]Lanzhou University, Lanzhou, Gansu, 730030, PR China, Shenzhen Eye Hospital, Shenzhen Eye Medical Center, Southern Medical University, No. 18, Zetai Road, Xiamihu Sub-district, Futian District Shenzhen, 518040, China

[b]Shenzhen Eye Hospital, Shenzhen Eye Medical Center, Southern Medical University, Shenzhen, 518040, PR China

[c]Lanzhou Huaxia Eye Hospital, Lanzhou, Gansu, 730030, PR China

***Corresponding Author: Wei Chi**

Abstract:
Age-related cataract (ARC) is driven by progressive oxidative damage and apoptosis in lens epithelial cells, yet the contribution of urban contaminants remains uncertain. 6PPD-quinone (6PPD-Q), an ozone-derived oxidation product of the tire antioxidant 6PPD, is widespread in urban environments and exhibits strong redox activity. Building on our analysis, we used a network toxicology workflow to explore its potential intersection with cataract biology. We predicted a consolidated set of 382 human protein targets and profiled gene expression in anterior lens-capsule transcriptomes from cataract versus control samples, identifying 856 significantly altered genes. Intersecting these datasets yielded nine candidates—AKT1, APAF1, AMD1, DHODH, GABRG2, GSR, MAOB, S100A9, and TRPA1—that formed a connected protein–interaction module enriched for FAD-dependent oxidoreductase activity, glutathione metabolism, arginine and proline metabolism, and apoptosis. Molecular docking supported direct interactions between 6PPD-quinone and all nine proteins, with binding free energies ranging from −6.1 to −9.9 kcal·mol^{-1}, and the strongest affinities for the mitochondrial oxidoreductases DHODH and MAOB. These systems-level findings outline a plausible mechanism whereby 6PPD-quinone disrupts lens redox homeostasis and cell survival signaling, generating testable hypotheses for cellular and in vivo validation and indicating a potential environmental contributor to lens aging.

Keywords: 6PPD-quinone; age-related cataract; network toxicology; oxidative stress; apoptosis; molecular docking

1. Introduction

Age-related cataract (ARC) is characterized by progressive clouding of the lens, resulting in visual impairment and blindness in older adults. It accounts for the majority of age-associated blindness globally (Cicinelli et al., 2023; Steinmetz et al., 2021). At the molecular level, ARC pathogenesis is driven by chronic oxidative damage to lens proteins and lipids, leading to protein aggregation and loss of lens transparency (Cvekl & Vijg, 2024; Ruiss et al., 2022; Wishart et al., 2021). In particular, oxidative stress triggers lens epithelial cell (LEC) apoptosis via caspase activation and disrupts redox homeostasis in the lens, for example by depleting glutathione and other antioxidants (Ruiss et al., 2022; Thompson et al., 2022). Defense pathways involving Nrf2, PI3K/Akt signaling, and antioxidant enzymes are known to protect LECs;

their failure contributes to cataract development (Liu et al., 2022; Rowan et al., 2021). For example, the PAK1/cleaved caspase-3 axis has been shown to mediate LEC apoptosis in ARC (Zhang et al., 2025). Recently, AKT1 has been identified as a key pro-oxidant factor in human cataract: silencing AKT1 in oxidatively stressed LECs reduced reactive oxygen species (ROS) and apoptosis (Huang et al., 2025). Collectively, these findings underscore that dysregulation of oxidative and apoptotic programs underlies age-related lens opacification (Cvekl & Vijg, 2024; Wishart et al., 2021).

Environmental factors, including contaminants that induce oxidative stress, may modulate cataract risk. One emerging pollutant of concern is 6PPD-quinone, the oxidized form of 6PPD, N-(1,3-dimethylbutyl)-N′-phenyl-1,4-phenylenediamine (Cao et al., 2022; Zoroufchi Benis et al., 2023). 6PPD is a ubiquitous rubber antioxidant used in tires to prevent ozone cracking; abrasion of tires releases 6PPD into the environment, where it readily oxidizes to 6PPD-quinone (6PPD-Q) (Lane et al., 2024; Zoroufchi Benis et al., 2023). The latter is highly stable and has been detected in urban runoff, sediments, ambient air, and even human blood and breast milk (Cao et al., 2022; Lane et al., 2024; Wan et al., 2024; Wu et al., 2024; Zhu et al., 2024). Notably, Tian et al. (2021) reported in Science that 6PPD-Q is acutely lethal to coho salmon at nanomolar concentrations, implicating it as a major cause of fish die-offs. The compound's environmental pervasiveness and potent bioactivity raise concerns about human exposure (Lane et al., 2024; Wan et al., 2024). Indeed, 6PPD-Q has been measured in human cerebrospinal fluid—with higher levels in Parkinson's patients than in controls—and was shown to induce mitochondrial ROS and exacerbate α-synuclein pathology in neurons (Fang et al., 2024). Together, these observations indicate that 6PPD-quinone can penetrate biological barriers and trigger oxidative stress in vivo (Fang et al., 2024; Wan et al., 2024).

Given the lens's sensitivity to oxidation, it is plausible that 6PPD-quinone exposure could influence cataract formation. However, to date no studies have directly examined 6PPD-Q in ocular tissues or cataract models. A recent aquatic-toxicology study found that 6PPD itself, rather than the quinone, disrupted thyroid signaling and eye development in zebrafish larvae, suggesting species- or endpoint-specific effects on ocular tissues (Chang et al., 2024). To address this knowledge gap, we employed a network toxicology approach to predict molecular targets and pathways by which 6PPD-quinone might impact ARC (del Giudice et al., 2024). Combined with molecular docking, this strategy has been applied successfully to decipher the mechanisms of diverse toxicants and xenobiotics at the systems level (Eberhardt et al., 2021). In the present study, we first predicted potential protein targets of 6PPD-quinone using chemoinformatics databases (e.g., SwissTargetPrediction and PharmMapper) (Daina et al., 2019; Wang et al., 2017) and identified differentially expressed genes (DEGs) from human cataract transcriptome data in the Gene Expression Omnibus (GEO) repository (Clough et al., 2024). Intersecting these datasets yielded candidate genes potentially affected by 6PPD-Q in cataract. Protein–protein interaction (PPI) analysis and hub-gene screening highlighted key nodes (Chin et al., 2014; Szklarczyk et al., 2023). Gene Ontology (GO) and Kyoto Encyclopedia of Genes and Genomes (KEGG) enrichment revealed predominant biological processes (Gene Ontology Consortium, 2023; Kanehisa et al., 2023). Finally, molecular docking of 6PPD-Q with selected targets was performed to evaluate binding affinity (Eberhardt et al., 2021). Through this pipeline, we aimed to uncover plausible molecular mechanisms linking 6PPD-quinone exposure to age-related cataract risk.

1. Materials and Methods

2.1 Study Design Overview

We integrated computational target prediction with human cataract transcriptomics to nominate candidate targets of 6PPD-Q and explored their biological context via PPI/association networks, GO/KEGG enrichment, and molecular docking. All URLs, software versions, and thresholds are provided at first mention; unless otherwise stated, tools were run with default settings.

2.2 Compound and in Silico Target Prediction

The chemical structure and SMILES of 6PPD-quinone (PubChem CID: 154926030) were retrieved from PubChem (https://pubchem.ncbi.nlm.nih.gov) (Wang et al., 2012). Putative human protein targets were predicted using three orthogonal web servers: Similarity Ensemble Approach (SEA, https://sea.bkslab.org; Keiser et al., 2007), SwissTargetPrediction (http://www.swisstargetprediction.ch; Daina et al., 2019), and PharmMapper (https://lilab-ecust.cn/pharmmapper; Liu et al., 2010). Target lists from the three sources were unioned and deduplicated, yielding 382 unique proteins for 6PPD-Q.

2.3 Human Lens Transcriptome Dataset and DEG Calling

We downloaded the GSE213546 dataset from NCBI GEO (https://www.ncbi.nlm.nih.gov/geo; Barrett et al., 2013), comprising anterior lens-capsule samples from 3 healthy controls and 3 patients with ARC on a common microarray platform. Raw data were normalized and analyzed using limma (Smyth, 2005). Differential expression was defined by $P < 0.05$ and $|\log_2 FC| > 0.2$, identifying 856 DEGs (413 up-regulated, 443 down-regulated) in ARC versus control.

2.4 Candidate Gene Intersection

The union of 6PPD-Q predicted targets and ARC DEGs was intersected to obtain disease-relevant candidates, yielding nine genes: TRPA1, S100A9, GSR, DHODH, MAOB, GABRG2, AMD1, AKT1, and APAF1.

2.5 PPI and Gene–Gene Association Analyses

To evaluate physical/functional relationships among candidates, we queried STRING (version 12.0; https://string-db.org; Szklarczyk et al., 2023) with Homo sapiens specified and a minimum required interaction score of 0.15 to build a PPI network. Hub genes were ranked by degree using cytoHubba within Cytoscape (Chin et al., 2014). In parallel, an association network was built with GeneMANIA (http://www.genemania.org; Warde-Farley et al., 2010) to visualize co-expression and pathway co-membership.

2.6 Functional Enrichment Analysis

GO and KEGG enrichment over the candidate set were performed using clusterProfiler (v4.10.0; Yu et al., 2012). $P < 0.05$ was considered significant; Biological Process, Cellular Component, Molecular Function terms and KEGG pathways were ranked by enrichment score (Ashburner et al., 2000; Kanehisa & Goto, 2000).

2.7 Molecular Docking

For each candidate target, experimentally determined protein structures were downloaded from the RCSB PDB (https://www.rcsb.org; Burley et al., 2017). The 3D structure of 6PPD-Q was obtained from PubChem and converted as needed from SDF/SMILES. Docking simulations were carried out with AutoDock Vina (Eberhardt et al., 2021). Receptor structures were prepared by removing co-crystallized ligands and water; receptor/ligand files were formatted for docking. When a canonical active site was known, the grid box encompassed that pocket; otherwise, a larger box covering the functional region was used. Binding affinity was reported as Vina score ($kcal \cdot mol^{-1}$); in line with network-toxicology docking screens, scores < -5.0 $kcal \cdot mol^{-1}$ were taken to support favorable binding (Yin et al.,

2020). Docking poses were visualized in PyMOL (Seeliger & de Groot, 2010).

2.8 ADME/Tox Property Profiling (Contextual Interpretation)

To contextualize systemic exposure potential, we profiled 6PPD-Q with SwissADME (http://www.swissadme.ch; Daina et al., 2017) and ADME Tlab 3.0 (https://admetlab3.scbdd.com; Fu et al., 2024). Reported descriptors included GI absorption, BBB permeability, plasma-protein binding, and cytochrome P450 inhibition probabilities. These metrics were not used for filtering but to aid biological interpretation in Discussion.

2. Results

3.1 In Silico Disposition and Physicochemical Profile of 6PPD-Quinone

Concordant outputs from SwissADME and ADMETlab 3.0 indicate an exposure pattern favorable to systemic distribution and tissue persistence. Gastrointestinal absorption is classified as high. Plasma-protein binding is very high at approximately 98.415%, implying a small free fraction yet prolonged residence in circulation. Blood–brain barrier permeability is predicted to be positive. On the metabolic axis, multiple cytochrome P450 isoforms show inhibition liabilities, suggesting constrained metabolic throughput; human liver microsomal stability (LM-human) is reported at 0.886, consistent with slow clearance. Medicinal-chemistry rule screens return single alerts in both PAINS and Brenk panels. Together, these features constitute an "easy absorption–high binding–slow metabolism" fingerprint that provides an exposure rationale for system-level interrogation in lens-relevant pathways. Key parameters are summarized in Table 1; the curated 2D structure appears in Figure 1.

Table 1. In silico ADME/T predictions for 6PPD-quinone from SwissADME and ADMETlab 3.0.

Target	SwissADME result	ADMETlab 3.0 probability
GI absorption	High	\
BBB permeant	Yes	\
PPB	\	98.415
LM-human	\	0.886
CYP1A2 inhibitor	Yes	0.997
CYP2C19 inhibitor	Yes	0.998
CYP2C9 inhibitor	Yes	0.013
CYP2D6 inhibitor	No	0.096
CYP3A4 inhibitor	Yes	0.969
CYP2B6 inhibitor	\	0.815
CYP2C8 inhibitor	\	0.999
PAINS	1 #alerts	\
Brenk	1 #alerts	\

Summary of key disposition and safety-relevant parameters, including GI absorption (High), BBB permeation (Yes), plasma-protein binding (PPB, 98.415%), human liver microsomal stability (LM-human, 0.886), major cytochrome P450 inhibition liabilities (e.g., CYP1A2, CYP2C19, CYP3A4), and medicinal-chemistry alerts (PAINS = 1; Brenk = 1).

Figure 1. Chemical structure of 6PPD-quinone (6PPD-Q).

Curated 2D structure of 6PPD-quinone (PubChem CID: 154926030) used for all in silico analyses.

3.2 Differential Expression Landscape in Age-Related Cataract Lens Epithelium

In the GSE213546 dataset, applying the prespecified thresholds ($P < 0.05$; $|\log_2$ fold change$| > 0.2$) yielded 856 DEGs, comprising 413 up-regulated and 443 down-regulated transcripts in the age-related cataract group versus control. The volcano plot depicts a broad and asymmetric perturbation field with clearly separated high-magnitude signals, indicating coherent transcriptome remodeling in cataractous lens epithelium. See Figure 2A.

3.3 Chemical–Disease Intersection: A Nine-Gene Interface

Predicted human targets of 6PPD-quinone were integrated from SEA, SwissTargetPrediction, and PharmMapper and deduplicated to 382 entries. Intersecting these with the 856 DEGs produced nine candidate genes, defining a minimal molecular interface between chemical perturbation and disease: AKT1, APAF1, DHODH, GSR, MAOB, AMD1, GABRG2, S100A9, and TRPA1. This overlap constitutes ~2.4% of all predicted targets and ~1.1% of all DEGs, indicating selective yet non-trivial convergence. Functionally, the panel covers survival–apoptosis control (AKT1, APAF1), flavin-dependent and thiol redox metabolism (DHODH, MAOB, GSR), polyamine biosynthesis and one-carbon flow (AMD1), inhibitory neurotransmission and chemical stress sensing (GABRG2, TRPA1), and a calcium-binding inflammatory mediator (S100A9). The intersection is illustrated in Figure 2B.

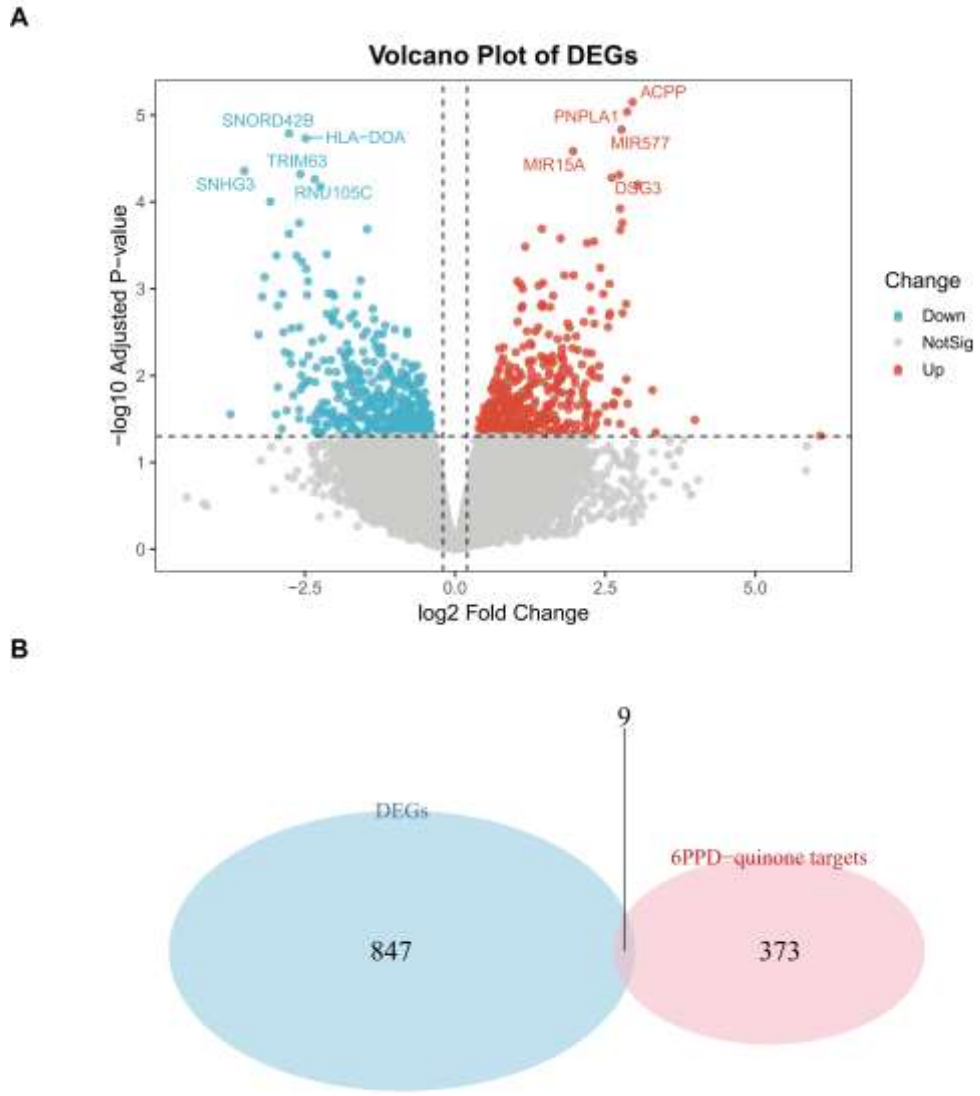

Figure 2. Transcriptomic landscape and chemical–disease intersection in ARC lens epithelium.
(A) Volcano plot of differentially expressed genes (DEGs) in GSE213546 (threshold: $P < 0.05$, $|\log_2 FC| > 0.2$).
(B) Overlap diagram between predicted 6PPD-quinone human targets (n = 382) and ARC DEGs (n = 856), yielding nine shared genes (AKT1, APAF1, AMD1, DHODH, GABRG2, GSR, MAOB, S100A9, TRPA1).

3.4 Protein–Protein Interaction Topology And Node Prioritization

A STRING network was constructed for the nine candidates in the human context using a minimum interaction score of 0.15, producing a single connected module. Degree-based ranking with cytoHubba in Cytoscape reveals a peaked topology in which a small subset of nodes carries most of the connectivity burden. A complementary GeneMANIA co-function map shows dense co-expression and shared pathway membership, with edges frequently annotated to oxidoreductase activity linked to NAD(P)H and to sulfur-group donors. This organization is consistent with lens pathology in which redox enzymes and cell-fate regulators act as leverage points for upstream chemical stress. See Figure 3A–B.

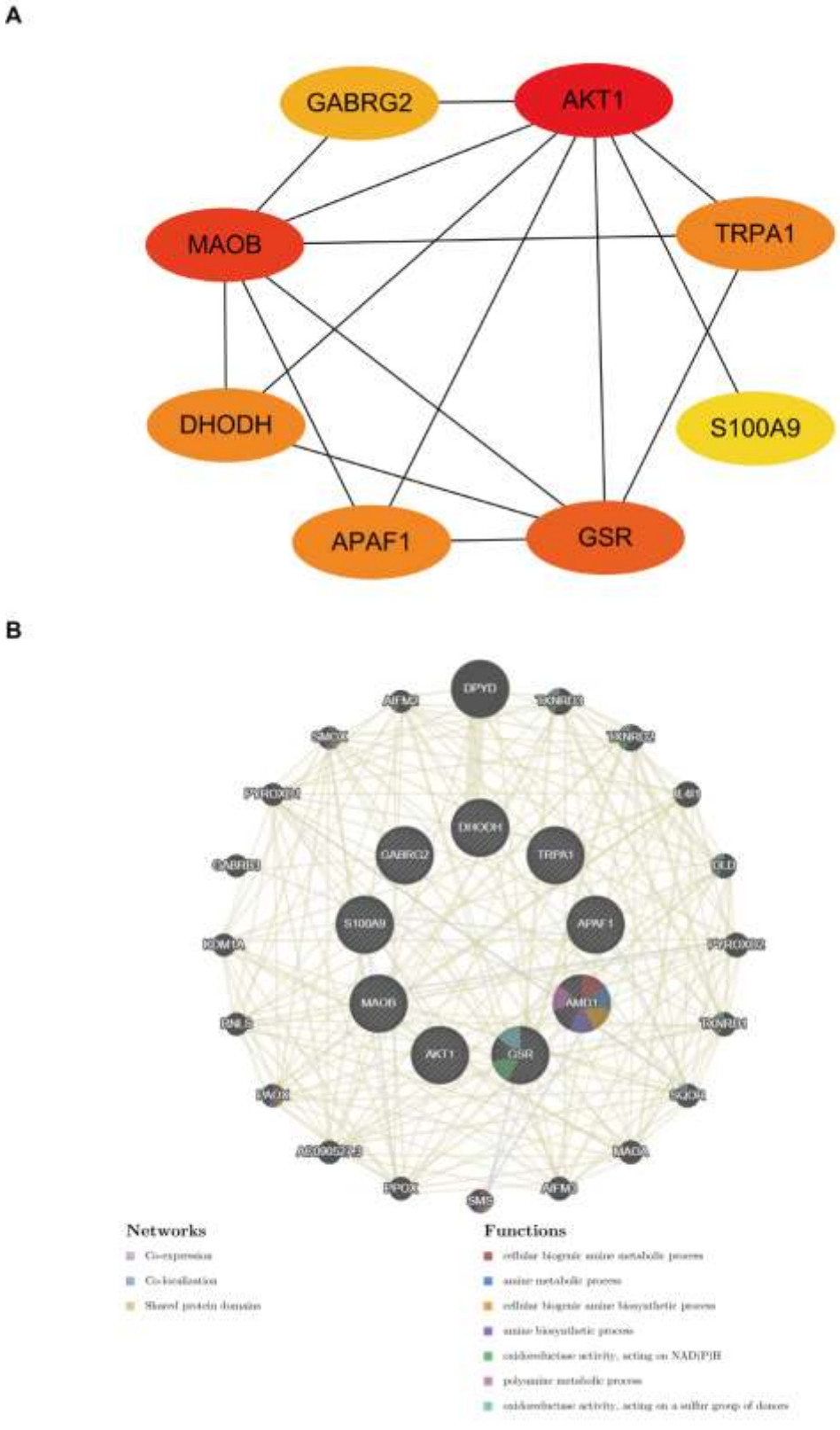

Figure 3. Network organization of the nine candidate genes.

(A) STRING protein–protein interaction (PPI) network (Homo sapiens; minimum required interaction score = 0.15) showing a single connected module.

(B) Node prioritization by cytoHubba (degree) and complementary GeneMANIA co-function associations highlighting redox enzymes and cell-fate regulators.

3.5 Functional Enrichment Outlines a Redox–Metabolism–Apoptosis Axis

Enrichment over the nine-gene set produced a compact and informative profile across Gene Ontology and KEGG. In GO we recorded 427 significant terms in total (Biological Process 358, Cellular Component 14, Molecular Function 55) under the prespecified threshold. Biological Process emphasizes stress and chemosensory programs; Cellular Component highlights the GABA_A receptor complex; Molecular Function is dominated by flavin adenine dinucleotide (FAD) binding, pinpointing the flavoproteins DHODH and MAOB. KEGG returns 25 significant pathways, headed by arginine and proline metabolism, consistent with AMD1-driven polyamine flux; additional signals span apoptosis, lipid-peroxidation-related routes, and oxidative processes. See Figure 4A–B.

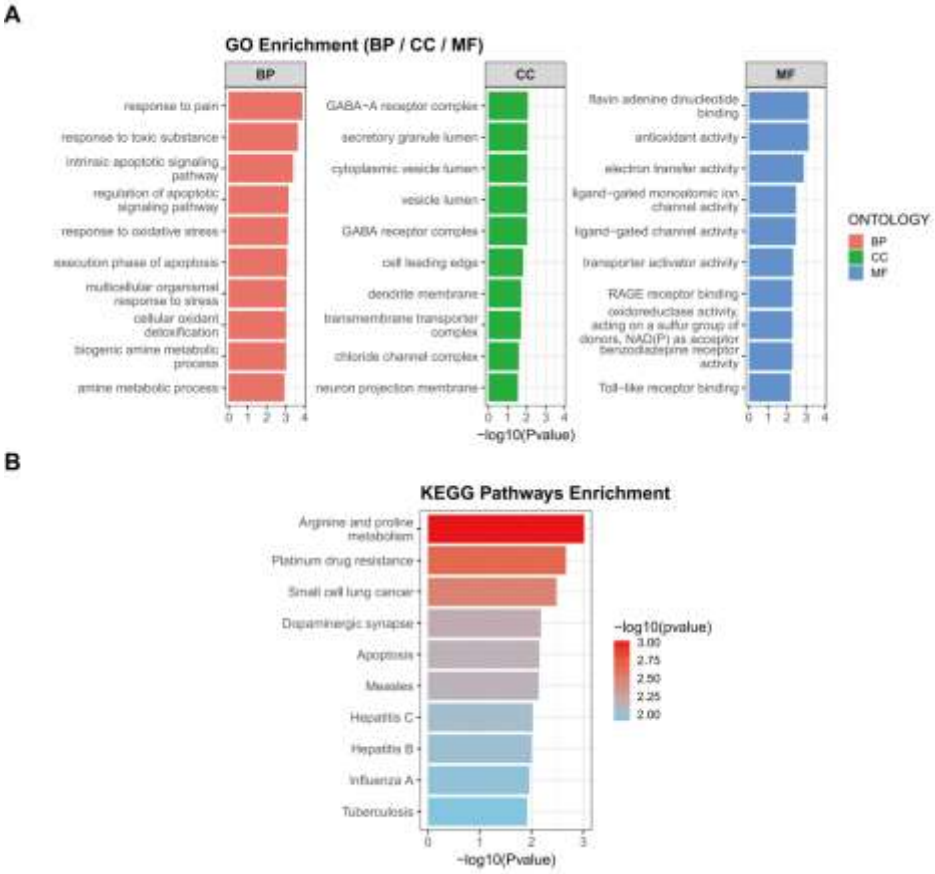

Figure 4. Functional enrichment profile of the nine-gene panel.

(A) Gene Ontology (GO) enrichment (Biological Process, Cellular Component, Molecular Function) highlighting stress/chemosensory programs, the GABA_A receptor complex, and FAD binding.

(B) KEGG pathways with significant enrichment, led by arginine and proline metabolism; additional signals include apoptosis- and oxidative-process-related routes.

3.6 Molecular Docking Supports Feasible Direct Engagement Across All Nine Targets

Molecular docking against experimentally determined structures of the nine proteins yielded AutoDock Vina binding energies from −6.1 to −9.9 kcal·mol^{-1}, all surpassing the predefined threshold of −5.0 kcal·mol^{-1}. Affinity ranking places DHODH (−9.9) and MAOB (−9.3) at the top, with APAF1 (−8.3) and GSR (−7.9) forming the next tier. AKT1 (−7.7) and TRPA1 (−7.6) occupy the mid-range, while AMD1 (−7.3), GABRG2 (−6.9), and S100A9 (−6.1) comprise the long tail. Representative complexes show

ligand occupancy within functional cavities or cofactor-associated grooves, with good shape complementarity and stabilizing hydrogen-bond and hydrophobic interactions. The affinity hierarchy coheres with the Molecular Function enrichment for FAD binding, pointing to mitochondrial flavin chemistry as a prioritized receptor landscape. Visualizations are compiled in Figure 5A–I.

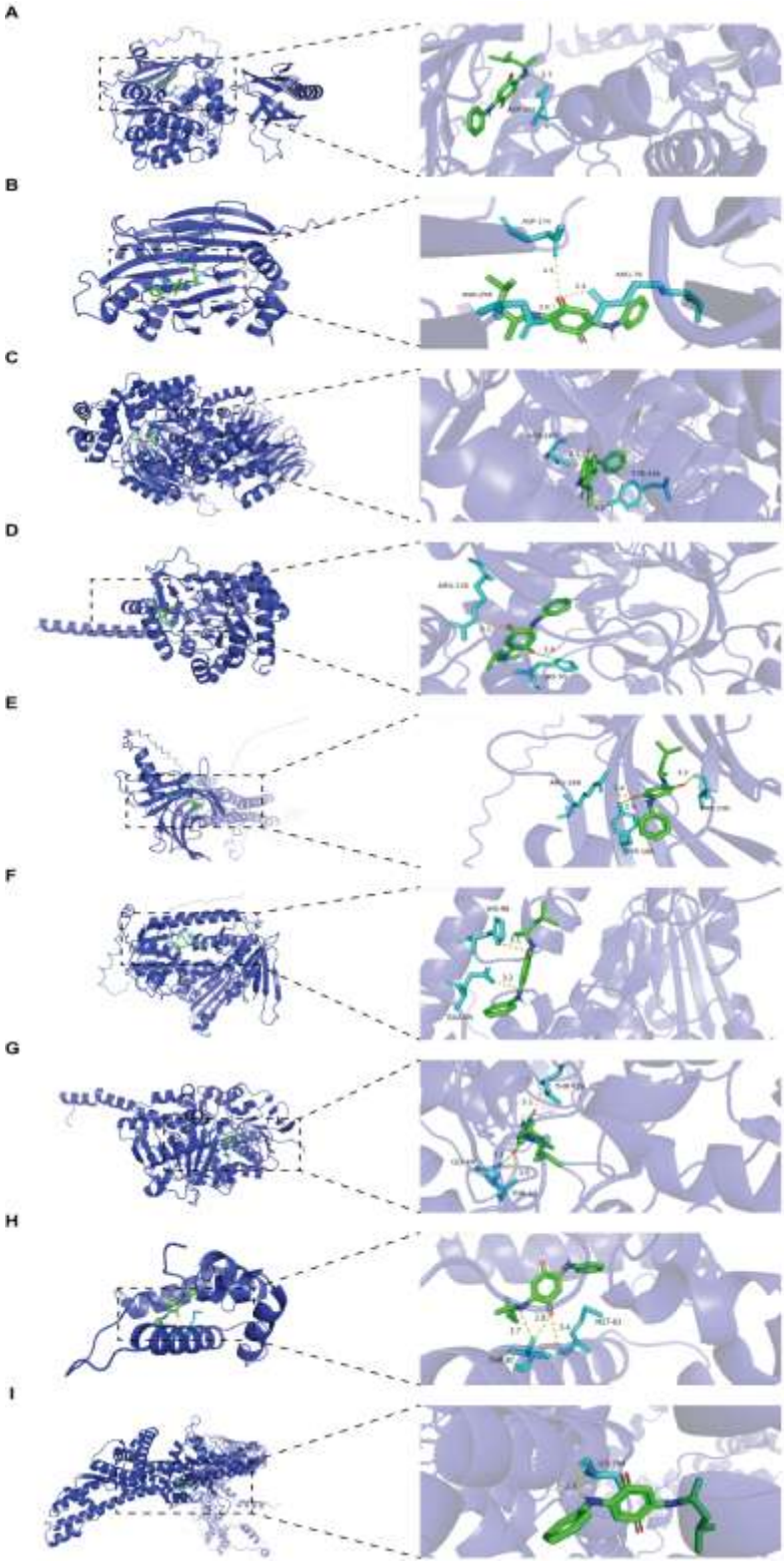

Figure 5. Molecular docking of 6PPD-quinone to nine targets.

(A–I) Representative docked complexes and best AutoDock Vina scores (kcal·mol^{-1}) for AKT1, APAF1,

AMD1, DHODH, GABRG2, GSR, MAOB, S100A9, TRPA1. Complexes show occupancy of functional cavities or cofactor-associated grooves with stabilizing hydrogen-bond and hydrophobic contacts. The affinity hierarchy (DHODH ≈ −9.9; MAOB ≈ −9.3; APAF1 ≈ −8.3; GSR ≈ −7.9; AKT1 ≈ −7.7; TRPA1 ≈ −7.6; AMD1 ≈ −7.3; GABRG2 ≈ −6.9; S100A9 ≈ −6.1) aligns with Molecular Function enrichment for FAD-binding proteins.

3.7 Cross-Layer Synthesis

Evidence from disposition profiling, transcriptomics, interaction topology, functional ontology, and docking is internally consistent. ADME/Tox features provide a plausible basis for 6PPD-quinone to reach ocular tissues at relevant exposure levels. The disease transcriptome establishes a background of oxidative stress, lipid imbalance, and apoptosis. The chemical–disease intersection focuses this backdrop onto nine candidates. The interaction network concentrates influence in redox enzymes and cell-fate regulators. Ontology highlights FAD-dependent chemistry and polyamine metabolism. Docking confirms energetically feasible binding at the corresponding protein pockets. Together, these layers support a testable working model in which 6PPD-quinone perturbs LEC redox homeostasis and lowers the threshold for apoptosis, accelerating the molecular cascade that precedes clinical opacification.

3. Discussion

This study assembled an integrative network toxicology chain—from disposition profiling through disease transcriptomics, chemical–disease intersection, protein-interaction topology, enrichment profiling, and docking—to propose a testable working model: 6PPD-Q may perturb redox homeostasis in LECs and lower the apoptotic threshold, thereby accelerating ARC. The argument aligns with the canonical molecular portrait of cataract—chronic oxidative stress, protein/lipid damage, mitochondrial dysfunction, and caspase-driven apoptosis (Cicinelli et al., 2023; Wishart et al., 2021; Thompson et al., 2022; Rowan et al., 2021).

Regarding exposure plausibility, the ADME/ADMET fingerprint—easy absorption, very high protein binding, slow clearance, and predicted BBB permeability—suggests favorable distribution and persistence in vivo. Independent lines of evidence indicate that 6PPD-Q is environmentally widespread and bioactive: reconnaissance monitoring across U.S. streams frequently detects 6PPD/6PPD-Q, and urban runoff can reach effect-relevant levels for sensitive species (Lane et al., 2024; Tian et al., 2021). Human biomonitoring has reported PPD-Q species, including 6PPD-Q, in urine and breast milk (Wu et al., 2024; Zhu et al., 2024), supporting a continuous exposure chain from roadway abrasion particles to the human body. These facts cohere with the disposition profile and provide the prerequisite to evaluate ocular risk, particularly under chronic or intermittent urban exposure.

On the disease background, analysis of GSE213546 (using the prespecified thresholds) identified 856 differentially expressed genes enriched for oxidative stress, lipid metabolism, and programmed cell death—an accurate molecular backdrop for ARC (Wishart et al., 2021; Thompson et al., 2022). Intersecting 382 predicted human targets of 6PPD-Q with these genes yielded nine candidates (AKT1, APAF1, DHODH, GSR, MAOB, AMD1, GABRG2, S100A9, TRPA1). This is not a generic list; rather, it compresses the disease "background" into a minimal interface along a redox–cell-fate axis: GSR sustains glutathione regeneration; MAOB and DHODH represent flavin-dependent redox chemistry; AKT1 and APAF1 gate survival and mitochondrial apoptosis; AMD1 couples

arginine/proline metabolism to polyamine and one-carbon flux; and TRPA1/GABRG2 point to stress sensing and inhibitory signaling that may fine-tune lens homeostasis. STRING/cytoHubba concentrates network "weight" on AKT1, GSR, MAOB, DHODH, and APAF1; GO/KEGG enrichment quantitatively highlights FAD binding (anchoring MAOB and DHODH) and AMD1, mirroring the literature-defined ARC axis of impaired glutathione cycling → mitochondrial ROS → caspase activation (Kanehisa et al., 2023; The Gene Ontology Consortium, 2023; Wishart et al., 2021; Thompson et al., 2022).

Molecular docking grounds the chemical–protein links at the structural level: all nine candidates meet the affinity screen (≤ −5.0 kcal·mol^{-1}), with DHODH and MAOB in the strongest tier and APAF1, GSR, and AKT1 following. Best poses occupy functional cavities or cofactor-adjacent grooves with stabilizing hydrogen-bond and hydrophobic contacts. The flavin preference in the affinity ranking echoes the GO signal for FAD binding and suggests prioritized perturbation of flavin chemistry and thiol cycling. Notably, Fang et al. (2024) showed that 6PPD-Q elevates mitochondrial ROS and exacerbates α-synuclein pathology in human neuronal models; by analogy, a mitochondrial–oxidative cascade is plausible in LECs as well.

At the level of node-specific interpretation, AKT1 and APAF1 form a bipartite survival–apoptosis pivot. Prior work indicates that AKT1 upregulation accompanies failure of stress resilience in LECs, while its silencing attenuates ROS and apoptotic propensity—consistent with feasible ligand engagement—whereas APAF1, once mobilized, drives the caspase-3 cascade, a recognized endpoint in cataractogenesis (Rowan et al., 2021; Wishart et al., 2021). On the redox side, reduced GSR capacity would compress the glutathione buffer; MAOB-mediated electron transfer and H_2O_2 by-products could escalate oxidative load; DHODH, which couples mitochondrial electron transport to pyrimidine synthesis, represents a dual gate for energy and biosynthesis that, if perturbed, could tilt cells toward death. This redox–fate axis maps well onto the known molecular frailty of the lens.

A third, tuning branch offers further mechanistic nuance. TRPA1, a canonical oxidative/electrophilic stress sensor, links redox perturbation to calcium influx and inflammatory signaling and aggravates retinal oxidative injury (de Araújo et al., 2020), resonating with our GO-BP signals for chemosensory/pain processes and suggesting a microcircuit of "stress sensing → Ca^{2+} influx → apoptotic priming" in LECs. GABRG2 implicates the GABA_A receptor complex; although its role in the lens remains to be defined, GABA receptors are reported in ocular tissues with calcium-signaling consequences (Cheng et al., 2015), hinting at potential crosstalk with ionic homeostasis and cell-volume regulation. AMD1-driven polyamine biosynthesis bridges arginine/proline metabolism with oxidative stress, inflammation, and proteostasis, aligning with the leading KEGG pathway in our analysis. Collectively, these "side branches" are not orthogonal to the main axis; rather, they amplify LEC vulnerability through resonance with redox and apoptotic circuitry.

When compared with existing toxicology, the picture favors slow, metabolism-centric stress over overt developmental toxicity for 6PPD-Q. Fang et al. (2024) support mitochondrial ROS amplification; in contrast, in zebrafish development 6PPD (not 6PPD-Q) provokes severe ocular damage with thyroid disruption (Chang et al., 2024), pointing to toxicant- and endpoint-specific differences. In mammalian lenses, therefore, 6PPD-Q is more likely to manifest as chronic metabolic/redox pressure—a pattern fitting the gradual, degenerative natural history of ARC (Tian et al., 2021; Cvekl & Vijg, 2024). We thus posit that under long-term low-dose or intermittent exposure, 6PPD-Q may

incrementally compromise flavin enzymes and glutathione cycling, eroding physiological redundancy and repair capacity in LECs and thereby accelerating aging trajectories.

We acknowledge the hypothesis-generating nature of this work. Target prediction and docking do not specify activation versus inhibition; the transcriptome reflects a relatively late disease state and likely includes secondary changes; tissue doses in human eye compartments remain unknown. Even so, the multilayer evidence prioritizes AKT1/APAF1 (apoptotic gating), GSR/MAOB/DHODH (redox–flavin metabolism), and TRPA1/AMD1/GABRG2 (tuning channels) as leverage points for validation. Accordingly, next steps should quantify mitochondrial function and glutathione redox metrics, reactive oxygen species, lipid peroxidation, and caspase activation in human LEC exposure models and chronic low-dose animal paradigms, coupled with target inhibition/overexpression to resolve causality; in parallel, real-world measurements of 6PPD-Q in ocular matrices (e.g., aqueous humor, lens tissue) should be correlated with opacification grading to inform risk assessment and prevention strategies (Kanehisa et al., 2023; The Gene Ontology Consortium, 2023; Cvekl & Vijg, 2024).

4. Conclusion

By integrating disposition profiling, disease transcriptomics, network analysis, enrichment, and structure-based docking, we define a nine-gene interface through which 6PPD-quinone (6PPD-Q) could influence age-related cataract. The convergence of signals on oxidative stress, apoptosis, and metabolic control provides a coherent, testable model: 6PPD-Q perturbs flavin-dependent redox chemistry (DHODH, MAOB) and glutathione recycling (GSR) while tipping survival–death gating (AKT1, APAF1), thereby lowering the resilience of lens epithelial cells and accelerating opacification. Additional nodes (TRPA1, AMD1, GABRG2, S100A9) suggest tuning pathways that may amplify redox and inflammatory vulnerability.

These results do not constitute causal proof; rather, they prioritize tractable targets and readouts for experimental validation. Immediate next steps include quantifying mitochondrial and glutathione metrics in lens epithelial models exposed to 6PPD-Q, perturbing the highlighted nodes to resolve directionality, and measuring ocular concentrations in real-world samples to establish exposure–effect relationships. As urban pollution persists alongside population aging, clarifying this chemical–disease linkage will be important for risk assessment and for developing targeted prevention strategies.

CRediT Authorship Contribution Statement

Zhuxuan Yan: Writing – original draft, Validation, Investigation, Methodology, Formal analysis, Funding acquisition. Hanrui Wang: Writing – review & editing, Validation, Investigation. Wei Chi: Writing – review & editing, Conceptualization, Methodology, Supervision, Funding acquisition. Zhenguo Yan: Validation, Conceptualization, Writing – review & editing, Resources.

Declaration of Competing Interest

The authors declare that they have no known competing financial interests or personal relationships that could have appeared to influence the work reported in this paper.

Acknowledgments

This study was supported by the Gansu Provincial Youth Science and Technology Fund Program (Grant No. 22JR11RA001); Key Project Fund of the National Natural Science Foundation of China (Grant No. 82230031); the Regional Innovation and Development Joint Fund of the National Natural Science Foundation of China (Grant No. U24A200954); the Key Special Project of "Cutting-Edge Biotechnology" in the National Key Research and Development Program of

China (Grant No. 2024YFC3406200); Sanming Project of Medicine in Shenzhen (Grant No. SZSM202411007); Guangdong Basic and Applied Basic Research Foundation, Regional Joint Fund Key Project (Grant No. 2023B1515120051); Shenzhen Bay Laboratory Basic Research Program (Grant No. SZBK2021080601009).

Appendix A. Supplementary Data

Supplementary Table S1 – Differentially expressed genes (GSE213546) with $\log_2$ fold change and P values (CSV); Supplementary Table S2 – Nine-gene intersection (AKT1, APAF1, AMD1, DHODH, GABRG2, GSR, MAOB, S100A9, TRPA1) with basic annotations (CSV); Supplementary Table S3 – Gene Ontology (BP/CC/MF) enrichment results with statistics (CSV); Supplementary Table S4 – KEGG pathway enrichment results with statistics (CSV); Supplementary Data S1 – SwissADME and ADMETlab 3.0 prediction matrices for 6PPD-quinone (XLSX); Supplementary Data S2 – STRING/GeneMANIA network edge lists and node attributes (XLSX); Supplementary Methods S1 – Docking settings (PDB IDs, chain IDs, grid centers and sizes, exhaustiveness/seed) and per-target contact residues (PDF).

Data Availability

Data will be made available on request.

References

1. Ashburner, M., Ball, C. A., Blake, J. A., et al. (2000). Gene Ontology: tool for the unification of biology. Nature Genetics, 25, 25–29. https://doi.org/10.1038/75556
2. Barrett, T., Wilhite, S. E., Ledoux, P., Evangelista, C., Kim, I. F., Tomashevsky, M., et al. (2013). NCBI GEO: archive for functional genomics data sets—update. Nucleic Acids Research, 41(D1), D991–D995. https://doi.org/10.1093/nar/gks1193
3. Burley, S. K., Berman, H. M., Kleywegt, G. J., et al. (2017). Protein Data Bank (PDB): The single global macromolecular structure archive. Methods in Molecular Biology, 1607, 627–641. https://doi.org/10.1007/978-1-4939-7000-1_26
4. Cao, G., Wang, W., Zhang, J., Wu, P., Zhao, X., Yang, Z., Hu, D., & Cai, Z. (2022). New evidence of rubber-derived quinones in water, air, and soil. Environmental Science & Technology, 56(7),4142–4150. https://doi.org/10.1021/acs.est.1c07376
5. Chang, J., Zhao, N., Zhang, L., Li, Y., Sun, Y., et al. (2024). 6PPD, not 6PPD-quinone, induced serious zebrafish eye damage with thyroid disruption. Environmental Science & Technology, 58(50),22076–22088. https://doi.org/10.1021/acs.est.4c11264
6. Cheng, Z.-Y., Sun, Y., Wang, Z., et al. (2015). GABA_Aα1 and GABA_Aρ1 subunits are expressed in cultured human RPE cells and GABA_A receptor agents modify intracellular Ca^{2+}. Experimental Eye Research, 132, 59–70. https://doi.org/10.1016/j.exer.2015.01.009
7. Chin, C.-H., Chen, S.-H., Wu, H.-H., Ho, C.-W., Ko, M.-T., & Lin, C.-Y. (2014). cytoHubba: identifying hub objects and sub-networks from complex interactome. BMC Systems Biology, 8(S4), S11. https://doi.org/10.1186/1752-0509-8-S4-S11
8. Cicinelli, M. V., Buchan, J. C., Nicholson, M., Varadaraj, V., & Khanna, R. C. (2023). Cataracts. The Lancet, 401(10374), 377–389. https://doi.org/10.1016/S0140-6736(22)01839-6
9. Clough, E., Barrett, T., Wilhite, S. E., Ledoux, P., Evangelista, C., et al. (2024). NCBI GEO: archive for gene expression and epigenomics data sets: 23-year update. Nucleic Acids Research, 52(D1),D138–D144. https://doi.org/10.1093/nar/gkad965
10. Cvekl, A., & Vijg, J. (2024). Aging of the eye: Lessons from cataracts and age-related macular degeneration. Ageing Research Reviews, 99,102407. https://doi.org/10.1016/j.arr.2024.102407

11. Daina, A., Michielin, O., & Zoete, V. (2017). SwissADME: a free web tool to evaluate pharmacokinetics, drug-likeness and medicinal chemistry friendliness of small molecules. Scientific Reports, 7,42717. https://doi.org/10.1038/srep42717
12. Daina, A., Michielin, O., & Zoete, V. (2019). SwissTargetPrediction: updated data and new features for efficient prediction of protein targets of small molecules. Nucleic Acids Research, 47(W1),W357–W364. https://doi.org/10.1093/nar/gkz382
13. de Araújo, D. S. M., Lima, M. H. M., et al. (2020). TRPA1 mediates damage of the retina induced by oxidative stress. Cell Death Discovery, 6, 73. https://doi.org/10.1038/s41420-020-02863-6
14. del Giudice, D., Albini, A., Noonan, D. M., & Carloni, S. (2024). Network toxicology: an integrative framework to decipher the toxicity of chemicals and mixtures. Advanced Science, 11(24),e2401037. https://doi.org/10.1002/advs.202401037
15. Eberhardt, J., Santos-Martins, D., Tillack, A. F., & Forli, S. (2021). AutoDock Vina 1.2.0: new docking methods, expanded force field, and Python bindings. Journal of Chemical Information and Modeling, 61(8), 3891–3898. https://doi.org/10.1021/acs.jcim.1c00203
16. Fang, J., Wang, X., Cao, G., Wang, F., Ru, Y., Wang, B., & Cai, Z. (2024). 6PPD-quinone exposure induces neuronal mitochondrial dysfunction and exacerbates α-synuclein pathology. Journal of Hazardous Materials, 465,133312. https://doi.org/10.1016/j.jhazmat.2023.133312
17. Fu, L., Shi, S., Yi, J., et al. (2024). ADMETlab 3.0: an updated comprehensive online ADMET prediction platform enhanced with broader coverage, improved performance, API functionality and decision support. Nucleic Acids Research, 52(W1), W422–W431. https://doi.org/10.1093/nar/gkae236
18. Gene Ontology Consortium. (2023). Gene Ontology knowledgebase in 2023. Genetics, 224(1),iyad031. https://doi.org/10.1093/genetics/iyad031
19. Huang, Y., Lyu, B., Tang, K., & Hu, K. (2025). Regulatory role of the AKT1/AMPK pathway in oxidative stress of lens epithelial cells in cataract patients. Sichuan Da Xue Xue Bao Yi Xue Ban, 56(3), 761–769. (PubMed ID: 40964109)
20. Kanehisa, M., & Goto, S. (2000). KEGG: Kyoto Encyclopedia of Genes and Genomes. Nucleic Acids Research, 28(1), 27–30. https://doi.org/10.1093/nar/28.1.27
21. Kanehisa, M., Furumichi, M., Sato, Y., Kawashima, M., & Ishiguro-Watanabe, M. (2023). KEGG for taxonomy-based analysis of pathways and genomes. Nucleic Acids Research, 51(D1), D587–D592. https://doi.org/ 10.1093/nar/gkac963
22. Keiser, M. J., Roth, B. L., Armbruster, B. N., Ernsberger, P., Irwin, J. J., & Shoichet, B. K. (2007). Relating protein pharmacology by ligand chemistry (SEA). Nature Biotechnology, 25(2),197–206. https://doi.org/10.1038/nbt1284
23. Lane, R. F., Smalling, K. L., Bradley, P. M., Greer, J. B., Gordon, S. E., Hansen, J. D., Kolpin, D. W., Spanjer, A. R., & Masoner, J. R. (2024). Tire-derived contaminants 6PPD and 6PPD-Q: Analysis, sample handling, and reconnaissance of United States stream exposures. Chemosphere, 363, 142830. https://doi.org/10.1016/j.chemosphere.2024.142830
24. Liu, S., Liu, Y., Tian, H., Li, J., & Wang, X. (2022). Protection of human lens epithelial cells from oxidative stress by KGF-2 via Nrf2/HO-1 and PI3K/Akt pathways. Oxidative Medicine and Cellular Longevity, 2022,6933812. https://doi.org/10.1155/2022/6933812
25. Liu, X., Ouyang, S., Yu, B., et al. (2010). PharmMapper server: a web server for potential drug target identification using

pharmacophore mapping approach. Nucleic Acids Research, 38(Suppl. 2), W609–W614. https://doi.org/10.1093/nar/gkq300

26. Rowan, S., Jiang, S., Francisco, S. G., Pomatto, L. C. D., Ma, Z., Jiao, X., Campos, M. M., Aryal, S., Patel, S. D., Mahaling, B., Riazuddin, S. A., Duh, E., Lachke, S., Hejtmancik, J. F., de Cabo, R., Fitzgerald, P., & Taylor, A. (2021). Aged Nrf2-null mice develop all major types of age-related cataracts. Investigative Ophthalmology & Visual Science, 62(15),10. https://doi.org/10.1167/iovs.62.15.10
27. Ruiss, M., Findl, O., & Kronschläger, M. (2022). The human lens: An antioxidant-dependent tissue revealed by the role of caffeine. Ageing Research Reviews, 79, 101664. https://doi.org/10.1016/j.arr.2022.101664
28. Seeliger, D., & de Groot, B. L. (2010). Ligand docking and binding site analysis with PyMOL and AutoDock/Vina. Journal of Computer-Aided Molecular Design, 24(5), 417–422. https://doi.org/10.1007/s10822-010-9352-6
29. Smyth, G. K. (2005). limma: Linear Models for Microarray Data. In R. Gentleman et al. (Eds.), Bioinformatics and Computational Biology Solutions Using R and Bioconductor (pp. 397–420). Springer. https://doi.org/10.1007/0-387-29362-0_23
30. Steinmetz, J. D., Bourne, R. R. A., Briant, P. S., et al. (2021). Causes of blindness and vision impairment in 2020 and trends over 30 years. The Lancet Global Health, 9(2), e144–e160. https://doi.org/10.1016/S2214-109X(20)30489-7
31. Szklarczyk, D., Kirsch, R., Koutrouli, M., Nastou, K., Mehryary, F., et al. (2023). The STRING database in 2023: protein–protein association networks and functional enrichment analyses for any sequenced genome of interest. Nucleic Acids Research, 51(D1), D638–D646. https://doi.org/10.1093/nar/gkac1000
32. Thompson, B., Davidson, E. A., Chen, Y., Orlicky, D. J., Thompson, D. C., & Vasiliou, V. (2022). Oxidative stress induces inflammation of lens cells and triggers immune surveillance of ocular tissues. Chemico-Biological Interactions, 355,109804. https://doi.org/10.1016/j.cbi.2022.109804
33. Tian, Z., Zhao, H., Peter, K. T., Gonzalez, M., Wetzel, J., Wu, C., et al. (2021). A ubiquitous tire rubber–derived chemical induces acute mortality in coho salmon. Science, 371(6525), 185–189. https://doi.org/10.1126/science.abd6951
34. Wan, X., Liang, G., & Wang, D. (2024). Potential human health risk of the emerging environmental pollutant 6PPD-quinone: current evidence and future perspectives. Science of the Total Environment, 949, 175057. https://doi.org/10.1016/j.scitotenv.2024.175057
35. Wang, X., Shen, Y., Wang, S., Li, S., Zhang, W., & Liu, G. (2017). PharmMapper 2017 update: a web server for potential drug target identification with a comprehensive target pharmacophore database. Nucleic Acids Research, 45(W1), W356–W360. https://doi.org/10.1093/nar/gkx374
36. Wang, Y., Xiao, J., Suzek, T. O., Zhang, J., Wang, J., Zhou, Z., Han, L., Karapetyan, K., Dracheva, S., Shoemaker, B. A., Bolton, E., Gindulyte, A., & Bryant, S. H. (2012). PubChem's BioAssay database. Nucleic Acids Research, 40(D1), D400–D412. https://doi.org/10.1093/nar/gkr1132
37. Warde-Farley, D., Donaldson, S. L., Comes, O., Zuberi, K., et al. (2010). The GeneMANIA prediction server: biological network integration for gene prioritization and predicting gene function. Nucleic Acids Research, 38(Web Server issue), W214–W220. https://doi.org/10.1093/nar/gkq537
38. Wishart, T. F. L., Flokis, M., Shu, D. Y., Das,

S. J., & Lovicu, F. J. (2021). Hallmarks of lens aging and cataractogenesis. Experimental Eye Research, 210, 108709. https://doi.org/10.1016/j.exer.2021.108709

39. Wu, X., Hu, J., Yuan, Z., Wang, S., & Tong, L. (2024). p-Phenylenediamines (PPDs) and PPD-quinones (PPD-Qs) in human urine and breast milk samples: Urgent need for focus on PPD-Qs and the establishment of health threshold criteria. Journal of Hazardous Materials, 480,136176. https://doi.org/10.1016/j.jhazmat.2024.136176
40. Yu, G., Wang, L.-G., Han, Y., & He, Q.-Y. (2012). clusterProfiler: an R package for comparing biological themes among gene clusters. OMICS: A Journal of Integrative Biology, 16(5), 284–287. https://doi.org/10.1089/omi.2011.0118
41. Zhang, Y., Li, X., Wang, Q., Zhao, H., & Chen, J. (2025). EGCG mitigates apoptosis of lens epithelial cells in age-related cataract via the PAK1/cleaved caspase-3 pathway. Current Molecular Medicine, 25,1269–1281. (PubMed ID: 39949100)
42. Zhu, J., Guo, R., Ren, F., Jiang, S., & Jin, H. (2024). Occurrence and partitioning of p-phenylenediamine antioxidants and their quinone derivatives in water and sediment. Science of the Total Environment, 914, 170046. https://doi.org/10.1016/j.scitotenv.2024.170046
43. Zoroufchi Benis, K., Behnami, A., Minaei, S., Brinkmann, M., McPhedran, K. N., & Soltan, J. (2023). Environmental occurrence and toxicity of 6PPD-quinone: A review. Environmental Science & Technology Letters, 10(10), 815–823. https://doi.org/10.1021/acs.estlett.3c00521